

First attempt to model numerically seismically-induced soft-sediment deformation structures – a comparison with field examples

Małgorzata BRONIKOWSKA^{1, *}, Małgorzata PISARSKA-JAMROŹY¹ and A.J. (Tom) VAN LOON²

¹ Adam Mickiewicz University, Geological Institute, B. Krygowskiego 12, 61-680 Poznań, Poland

² Shandong University of Science and Technology, College of Earth Science and Engineering, Qingdao, China

Bronikowska, M., Małgorzata Pisarska-Jamroży, M., Van Loon, A.J. (Tom) 2021. First attempt to model numerically seismically-induced soft-sediment deformation structures – a comparison with field examples. *Geological Quarterly*, 2021, 65: 60, doi: 10.7306/gq.1629



No numerical model has thus far addressed seismites, even though seismites are frequently used for the reconstruction of seismic events in the geological past. This is the more remarkable since the boundary conditions which have to be fulfilled for the development of seismites have also been estimated only empirically. The present contribution is a first attempt to model numerically the soft-sediment deformation structures caused by the passage of S-waves through near-surface sedimentary layers. The simulations are based on the so-called pressure tube model and the iSALE2D program. We modelled a seismic S-wave with six different vertical velocities, ranging from 1.6 to 2.6 m · s⁻¹, passing through sediments with different densities and porosities in a sedimentary succession from the surface down to a depth of 10 m. The modelled soft-sediment deformation structures (load casts, flame structures, injection structures and sedimentary volcanoes) show similar geometries and sizes as those known from laboratory experiments and field studies. The geometry, size and type of these structures depend on the sediment properties and on the initial pressure used as a trigger mechanism, rather than on S-wave velocity. In contrast, the depth of the seismites appears to depend strongly on the S-wave velocity.

Key words: numerical modelling, seismic waves, wave propagation, seismites, soft-sediment deformation structures, load casts, injection structures.

INTRODUCTION

Seismically-induced soft-sediment deformation structures (SSDS) are caused by S-waves travelling through unconsolidated sediments (Rossetti, 1999) and are linked with liquefaction and fluidization processes. The SSDS can originate in water-saturated, unconsolidated sediments if an earthquake has a sufficiently large magnitude to trigger liquefaction ($M \geq 4.5$; Marco and Agnon, 1995; $M \geq 5.0$: Atkinson et al., 1984; Rodríguez-Pascua et al., 2000). Liquefaction reduces the shear strength of the water-saturated sediments, resulting in changing intergranular contacts (Allen, 1982; Obermeier, 1996; Vanneste et al., 1999; Owen and Moretti, 2011), and in plastic behaviour of the sedimentary mass (Van Loon et al., 2020). Liquefaction is restricted to depths of <10 m below the sedimentary surface, commonly <2 m or even a few decimetres.

The passage of a seismic shock wave through a sufficiently susceptible sedimentary layer causes soft-sediment deformation structures (SSDS) throughout the layer as far as the S-wave has not lost too much energy. The deformed layer is

called a “seimite” (Seilacher, 1969). Seismites have commonly a lateral extent up to 40 km from the epicentre (Galli, 2000), though this distance depends on the properties of the affected sediments and of the magnitude of the triggering earthquake. It is widely accepted that seismites can be easily formed in almost cohesion-less sands with a relatively high silt content (e.g., Moretti et al., 1999), for instance in lacustrine, marine, and fine-grained fluvial sediments (Alfaro et al., 1997; Hoffmann and Reicherter, 2012; Van Loon and Pisarska-Jamroży, 2014; Pisarska-Jamroży et al., 2018, 2019a, b).

A problem with the recognition of seismites is that strongly deformed layers intercalated between non-deformed layers can also have another origin (e.g., slumping). Among the various criteria that have been proposed for the recognition of seismites (Obermeier et al., 1990; Obermeier, 1996, 2009; Rossetti, 1999; Wheeler, 2002; Hilbert-Wolf et al., 2009; Owen and Moretti, 2011; Van Loon et al., 2016, 2020; Pisarska-Jamroży and Woźniak, 2019), the most commonly adhered to nowadays (Van Loon et al., 2016) is the presence of a combination of at least several of the following characteristics:

- alternating deformed and undeformed layers;
- lateral continuity of SSDS within the deformed layers;
- a wide variety of chaotically-distributed SSDS within the deformed layers;
- the lack of indications for other deformational mechanisms;
- a morphology of the SSDS that is consistent with those in undisputed seismites and in experimentally produced “seismites”;

* Corresponding author, e-mail: malgorzata.bronikowska@amu.edu.pl

Received: August 19, 2021; accepted: November 22, 2021; first published online: December 30, 2021

– a clear spatial association with features that may cause seismic S-waves (e.g., faults or active volcanoes).

Among the wide variety of SSDS within seismites, examples representing plastic and brittle behaviour (commonly accompanied by structures indicating fluidisation) occur that developed during the same deformational event (Rossetti et al., 2011; Pisarska-Jamroży and Woźniak, 2019). The presence of fluidised features (escape structures, clastic dykes, sand or silt volcanoes, pillar and vein structures, dish structures) indicates overpressure in the sediment (Doughty et al., 2014). Brittle deformations such as broken-up layers result from a sudden increase of the pore-water pressure. The development of structures indicating loading in a plastic state such as load casts, pseudonodules and flame structures reflects instable density gradients within the sediment, but loading also requires liquefaction and/or fluidisation of the underlying layer (Moretti and Ronchi, 2011; Belzyt et al., 2021).

The main objective of the present contribution is to present a relatively simple method for the numerical modelling of seismites, which model is validated by comparison with field observations. The results can increase the insight into the reconstruction of the sediment properties and earthquake characteristics.

METHODS

The present contribution presents a numerical model that helps understand the genesis of seismites. Each numerical model has some limitations; those of our model are detailed in Section: *Methodical approach – limitations* before the description of the model (Section: *A new approach – model description*) in order to make the various chosen steps understandable. Subsequently, the setup of the simulations is detailed (Section: *Setup of the simulations*).

METHODICAL APPROACH – LIMITATIONS

Numerical modelling of the origination of seismites poses a significant technical challenge for several reasons. First, all field observations suggest their occurrence at some distance from the epicentre of an earthquake (Galli, 2000), but the epicentre can, as a rule, not easily be located in the case of ancient seismites. Moreover, the S-wave velocity and the specific sediment properties at the time of the formation of an ancient seimite are not known, which largely increases the number and size of possible numerical errors. In addition, almost all widely used numerical models are based on the wave equation for a non-disturbed medium, due to some mathematically impossible calculations of wave motion in a disturbed sediment (e.g., Meada et al., 2017; Peng and Wang, 2019; Li et al., 2020), while those which address the irregularities in media (Jefeeris and Been, 2015; Boulanger and Ziotopoulou, 2017) do not include the development of SSDS in the final result, because of the enormous complexity of such numerical solutions. The main focus of such studies addresses the S-wave front velocity, neglecting the effect of the interaction of the seismic wave with the sediment below. Such models can well predict the effects of an earthquake, but they are useless for seimite modelling.

Another obvious problem in the numerical modelling of seismically-induced SSDS is the change in size and complexity of these deformations with increasing distance from the epicentre. Actual or experimentally produced SSDS tend to be relatively small (commonly millimetres to several decimetres: e.g., Owen, 1996; Moretti et al., 1999; Moretti and Sabato, 2007), partly be-

cause they are mostly located several kilometres away from the related earthquake epicentre (see Galli, 2000). Consequently, the resolution of modelled seismites has to be very high, which is not feasible at such a large distance. The computational cost of a model with a sufficiently high resolution would certainly be unreasonably high, while the numerical error would still be too large. The only solution for this problem is using a model that deals with a limited areal extent of the sediment, with initial conditions that can be computed with programs addressing the propagation of the seismic wave, and that are specific for a given distance from the epicentre.

Last but not least, the key processes and main agents during seimite formation are liquefaction and fluidisation of the sediment. Liquefaction occurs when the sediment strength is significantly reduced by the shear stress induced by a seismic wave. The cohesionless sediment gains mobility, and in consequence starts to move in the direction of least resistance. Such a movement causes an upward pressure, which sets the sediment in motion (Seed and Idriss, 1971). However, many issues related to liquefaction, such as the water content and the properties of the sediment during deformation are still unknown. Fluidisation can severely damage buildings and even result in collapse. Therefore, it is not surprising that the main focus in liquefaction/fluidisation research thus far was on sand behaviour during and immediately after these processes, rather than on the influence of this mechanism on the formation of SSDS (e.g., Vaid and Thomas, 1995; Andrus and Stokoe, 1997; Youd and Idriss 2001; Rahman and Lo, 2014; Rahman et al., 2020).

Although empirical functions and numerical modelling addressing the sediment liquefaction potential are very accurate and validated against abundant field and experimental data, numerous cases are known which are inconsistent with the above empirical laws. An accurate description of the liquefaction mechanism is, however, beyond the scope of the present contribution, and the above considerations are therefore meant only to inform the reader that the lack of exact theoretical models of this process should be taken into account where the possibilities of seimite modelling are discussed.

A NEW APPROACH – MODEL DESCRIPTION

Accurate seimite modelling requires a new approach avoiding all difficulties mentioned above. Our new model does so: it focuses primarily on the seismites themselves, while the sediment properties, the S-wave velocity and the shear stress required for sediment motion are assumed to be known. The model setup is designated to meet the liquefaction criteria so that the liquefaction process can be addressed, while the simulated sediments are chosen in such a way that they have the properties that best fit liquefaction. Because a high resolution is required, we simulate the passage of the vertical velocity component of the S-wave through a narrow (0.6 m) section of sediment (called “tube” in the following) from the surface down to a depth of 10 m. Such a setting of the model pretends that the simulated seismites develop where the vertical wave velocity is much higher than the horizontal one, which is assumed in our model to be negligible. These assumptions are easily validated because seismically-induced SSDS form due to shear stresses related to a vertical pressure (Seed and Idriss, 1971). The imaginary sediments used for the simulations have a strength that equals the strength of water-saturated sand, with a water content of 25%, and porosities of 15, 20, and 25%; further details are provided in Section: *Setup of the simulations*.

The simulations are conducted using the iSALE2D shock physics hydrocode (Wünnemann et al., 2006), which was origi-

nally designated to study an impact-related phenomenon (see Section: Setup of the simulations). The ISALE2D code allows simulating a water-saturated medium only by adding water to the analytical equation of state (ANEOS) table, which excludes any changes during the program run. In other words, the water content in the sediments remains constant during the entire simulation procedure, and is fixed in the computational material matrix.

This disadvantage of the model is not exceptional: a situation during which all water is expelled from the water-saturated sediment must be very rare: no seismites are known that show clear evidence of such a process. Moreover, it is the water content that significantly influences the strength of sediment. This holds for both actual and simulated seismites, which implies that this highly important aspect is addressed by our model in an adequate way.

It is worth noticing that the artificial numerical sediments that we use for our simulations are not only uniform, but are also assumed to give an ideal response of the sediment to the vertical pressure related to the S-wave velocity. Actual sediments often contain a discrete lamination, or other forms of discontinuity and density differences, which make them far less predictable. Consequently, naturally formed SSDS may differ from the modelled ones. This limitation, which is inherent to every numerical model, does not really influence the results presented here. The energy of the S-wave velocity is so high that the influence of discrete discontinuities in the medium on the final shape and size of the SSDS can be neglected. During the very short time interval, during which the S-wave with its typical velocity erases most of the discrete density differences, the vertical energy (and pressure) can be considered as constantly very high. In consequence, the wave does not “react” to discrete laminations or other irregularities while it passes a narrow sediment section (the tube).

SETUP OF THE SIMULATIONS

All simulations have been conducted using the iSALE2D code, which is based on a hydrocode solution algorithm (Amsden et al., 1980). It was originally developed for studies on hypervelocity impact cratering (Collins et al., 2004; Wünneman et al., 2006), but it can be applied to our study because it includes an elasto-plastic constitutive model, fragmentation models, various equations of state, a strength model and a porosity-compaction model. It has been benchmarked against other hydrocodes (Pierazzo et al., 2008) and validated against experimental data (Pierazzo et al., 2008; Davison et al., 2011; Miljković et al., 2012).

As the material (= sediment) for our simulations, we used an imaginary wet sand described by an analytical equation of state (ANEOS) as a mixture of quartz sand (75%) and water (25%) (yellowish in Figs. 1 and 2) and dry sand (brownish in Figs. 1 and 2) described by ANEOS as quartz. It is worth noticing that this choice of materials and their sedimentary succession was made mainly to address the density and small strength differences of successive layers, which are crucial for liquefaction. The simulated dry sand has a lower density and higher strength, which allows the passing S-wave to disperse during the contact with the less dense wet layer (see Fig. 3).

Two layers of sediment with the same physical properties cannot visibly interact with each other: only the discontinuity at the contact zone between two different layers can cause wave dispersion and, in consequence, the development of deformation structures. Numerous trial simulations have confirmed that the differences in the response of these two materials to high pressure caused by a propagating shock wave are insignificant. However, differences in densities and strength between suc-

cessive layers must be addressed in the model setup in order to develop seismites.

In our simulation, an S-wave passes a sedimentary column (the 10-m deep tube) with an initial setup reflecting an ideal succession of alternating wet and dry sands. The porosity and density of the sediment are constant and do not vary with depth. This can be considered as valid for depths to some 12 m. The shear strength and other parameters influencing the response of the sediment to high pressure changes for wet/dry sand vary with depth due to the overburden weight. These changes are, however, very small and can be considered as negligible.

The reaction of both the wet and dry sands to a high pressure is described by a strength model that has proven accurate for unconsolidated sediments and that is widely used in studies and laboratory impact experiments (Wünneman et al., 2006). The mixture of water and quartz sand grains, as well as dry sand contains randomly distributed pores which are assumed to constitute 15, 20 and 25% by volume, respectively (see Figs. 1 and 2). These pores become reduced in size during the passage of an S-wave (due to resulting compaction) but the pores (and consequently also the reduction in their sizes) are too small to be visible in Figures 1 and 2.

The resolution of each simulation is 3 cm, while the high-resolution grid consists of 200 horizontal and 4000 vertical cells. The combined grid of high-resolution cells forms a 10 m high and 0.6 m wide sedimentary succession (the above-mentioned “tube”, which is connected with a vertical plane ending above the surface and which is used as the trigger mechanism for the pressure related to the vertical component of the S-wave velocity: see Fig. 1). This vertical plane has, in the various simulations, an initial velocity of 1.6, 1.8, 2.0, 2.2, 2.4 and 2.6 $\text{m} \cdot \text{s}^{-1}$, which corresponds to the surface acceleration commonly determined for modern earthquakes. The simulation run begins when the sediment above the surface starts to move with the given velocity, starting a shock wave which travels down through the sediment tube.

In our model, the main focus is on developing SSDS. Therefore we simulate only a very narrow (0.6 m) section (the “tube”) in which the S-wave interacts with the sediment.

RESULTS

A higher S-wave velocity (the modelled velocities range from 1.6 to 2.6 $\text{m} \cdot \text{s}^{-1}$) is found to cause more compaction of the modelled sedimentary succession (black in Fig. 1). The compaction related to the propagation of the S-waves depends on the type of sediment but not on the S-wave velocity. In dry sands (yellowish in Fig. 1), compaction is almost constant (~10%); it is neither related to the S-wave velocity nor to the initial porosity (i.e., 15, 20 or 25%). Compaction in the water-saturated sands (brownish in Fig. 1) after the passage of the shock wave reaches 40%; it is not related to the S-wave velocity but increases (from 33 to 45%) with an increase of porosity from 15 to 25%. No clear relationship has been found between the compaction and the depth of the sand.

It is worth noticing that all used simulations end when the S-wave reaches a depth of 10 m, so as to avoid numerical errors related to wave reflection. During actual seismic events, when an S-wave travels through a porous medium, the pores become pressed or even disappear, and the sediments become compacted by the stress related to the shock-induced pressure. Almost immediately afterwards, however, the sediment undergoes relaxation, rising again after the short phase of compaction, due to its plasticity. In the simulations presented

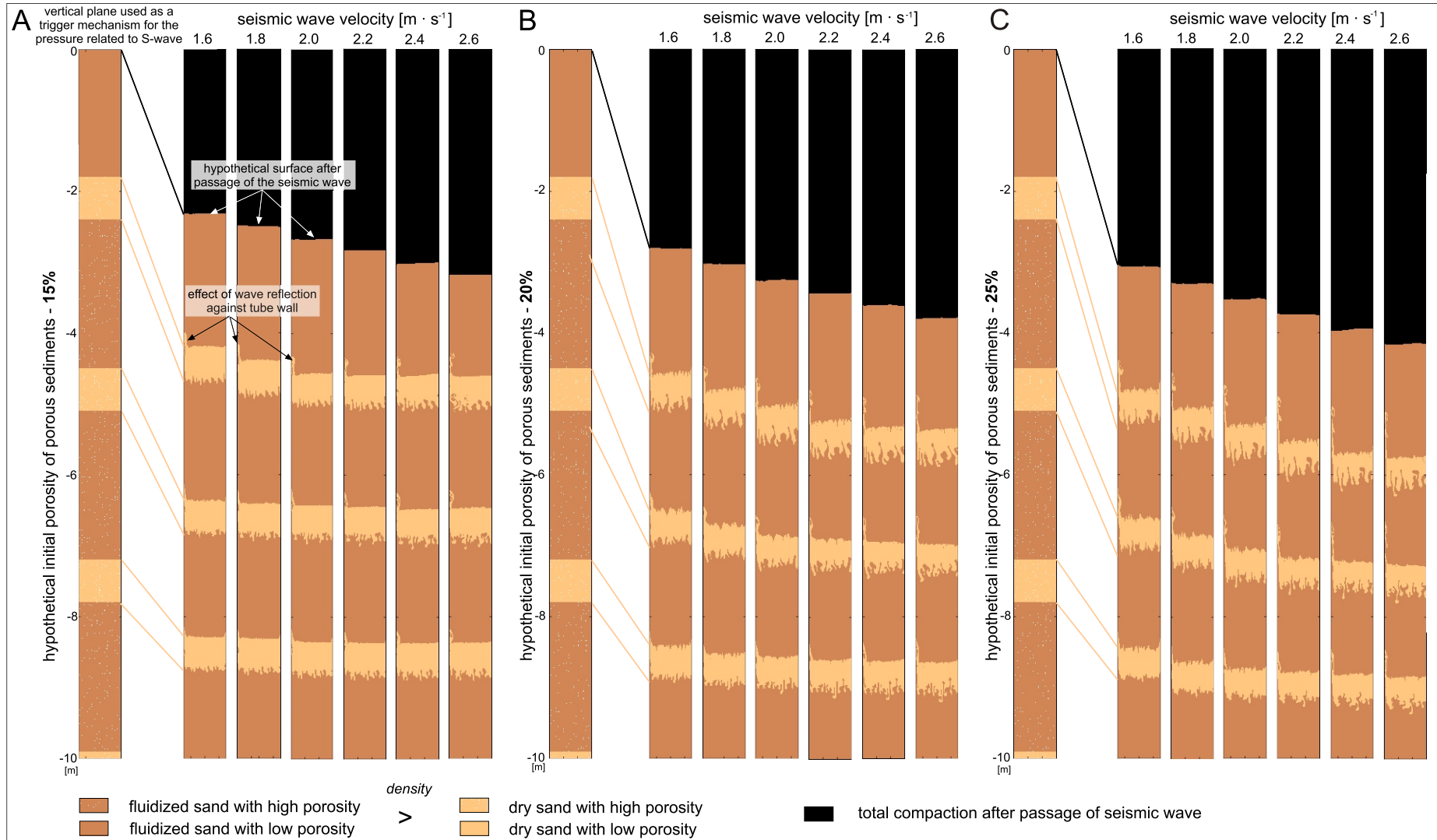


Fig. 1. Hypothetical sedimentary succession in a tube of 10 m deep and 0.6 m wide, with sediments of different porosities (A – 15%, B – 20%, C – 25%)

The model indicates that the passage of an S-wave results in compaction and the development of soft-sediment deformation structures (SSDS); the total compaction depends mainly on the velocity of the S-wave, whereas the size of the SSDS depends mainly on the original porosity of the sediment; note that the imaginary wall of the tube causes reflections of the S-wave, which results in the model in small disturbances close to this wall, which will not occur under actual conditions

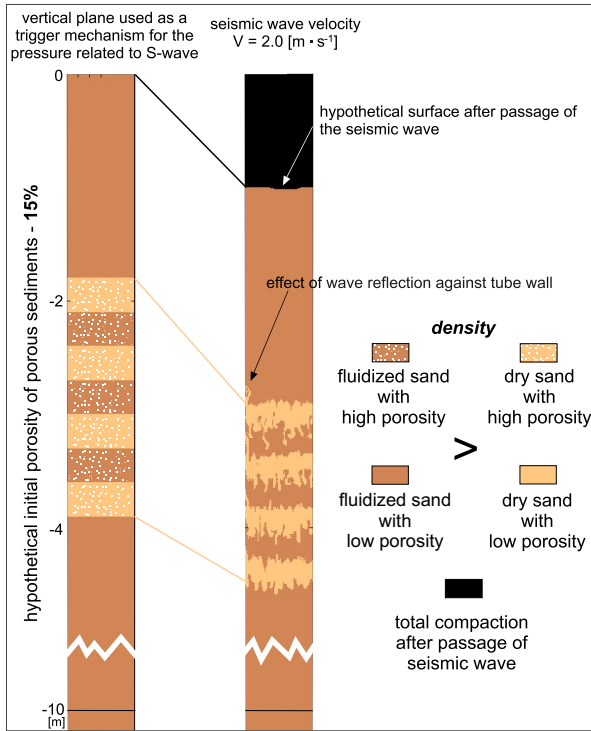


Fig. 2. Simulation of the upper part of a hypothetical sedimentary succession of 10 m thick, consisting of stratified sands with a porosity of 15%, affected by an S-wave that passed with a velocity of $2 \text{ m} \cdot \text{s}^{-1}$

Compaction occurred and SSDS developed; similar simulations were carried out for all initial porosities of the sediment and for all wave velocities indicated in Figure 1

here, this relaxation does not occur: the setup does not allow relaxation of the sediments after they have been exposed to the high vertical pressure, which definitely overestimates the compaction values found. Although the relationship between the wave velocity, sediment properties and compaction values are valid, the compaction values presented here should be considered as the maximum ones that may be reached. Also the deformed surface in Figure 2 should be interpreted with caution. The upper surface of the sediment is in our simulations located in the area of the computational grid, where the numerical errors are highest. It is probably true that some of the features located there result from interaction of the S-wave with the empty computational cells; this cannot be considered as a proper physical situation.

The size and shape of seismically-induced SSDS hardly depend on the S-wave velocity. On the other hand, the depth at which SSDS originate depends strongly on it: this depth increases with increasing S-wave velocity, which is particularly clear for relatively porous sands (compare the SSDS in Fig. 1 between sub-figures A, B and C). It appears also that the SSDS in seismites at comparable depths are more complex and more chaotically distributed in more porous sands than in less porous sands (Fig. 1). The reason is that a higher wave velocity causes more mobilization of the particles in liquefied sands (brownish in Fig. 1) and that, consequently, the developing SSDS move farther downwards. This finding is of great importance because it allows the reconstruction of the propagation direction of the seismic S-wave: a distinct downward shift of the SSDS in a lateral direction always roughly indicates the resultant of the maxima of the wave energy (which can be expressed in terms of velocity), whereas an upward shift indicates the minima of the wave energy (Figs. 1 and 2).

The size of the SSDS depends only slightly on the S-wave velocity in sands with a low (15%) porosity, although the sands

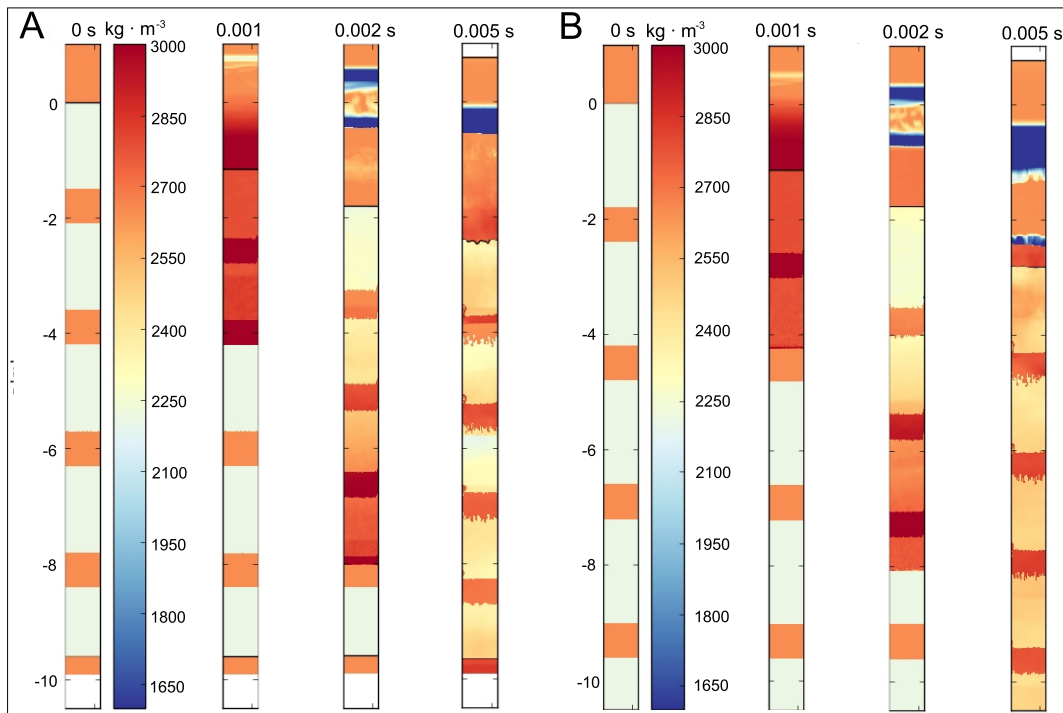
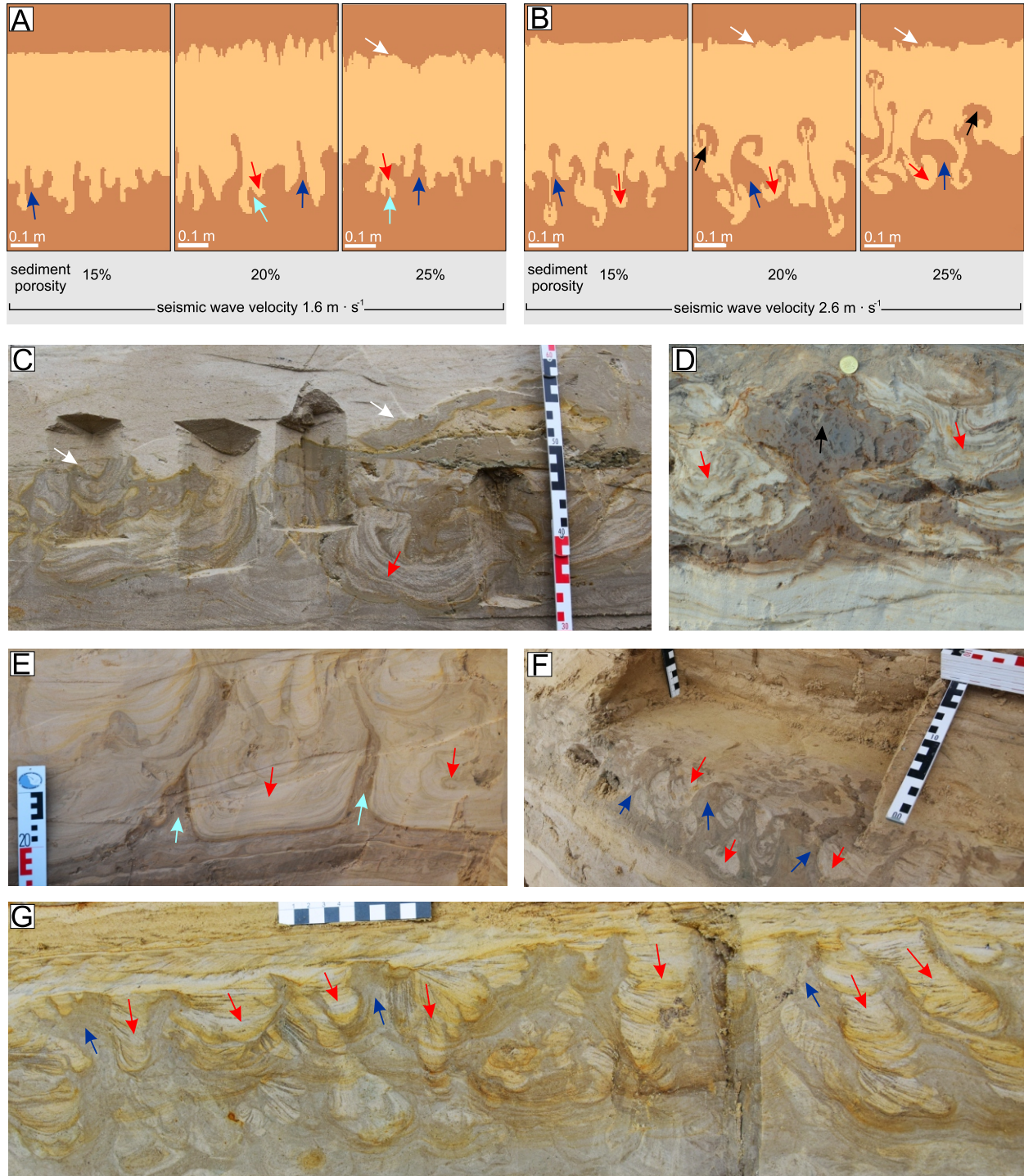


Fig. 3. Simulation of the effect of a passing S-wave with a velocity of $2 \text{ m} \cdot \text{s}^{-1}$ on two sedimentary successions with different initial vertical density distributions (A and B) before passage (first tube) and after 0.1, 0.2, and 0.5 s

that are least susceptible to compaction develop larger and more pronounced SSDS with increasing S-wave velocity. This is probably because a low porosity results in a less diminishing pressure. When an S-wave travels through the sands, it loses energy each time that it passes and reduces the size of a pore. The lateral differences in the energy of a wave (which is related to its velocity) at the given depth are therefore larger for low-porosity sands (due to less dispersion) than for high-porosity ones. This

energy loss is proportional to the initial velocity, so that a higher initial energy of a wave will result in more dispersion.

The geometry and size of the modelled SSDS are consistent with actual seismically-induced SSDS (Fig. 4). The size of the modelled SSDS varies from a few up to 25 cm. Simulations of the S-wave passage through a relatively thin succession of alternating dry and liquefied sands show therefore in our model alternating deformed and undeformed layers (Figs. 2 and 5A).



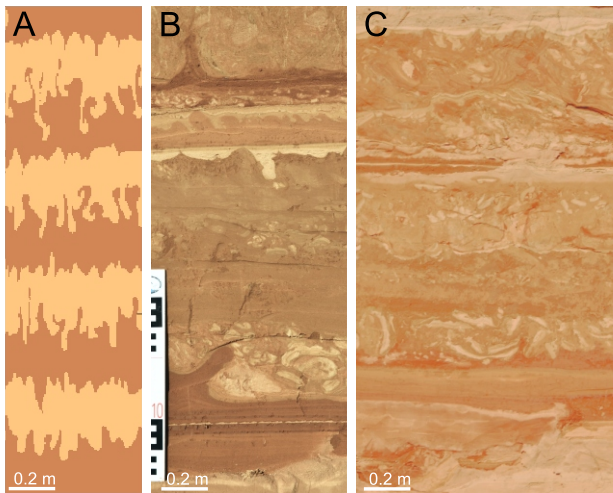


Fig. 5. Comparison of modelled SSDS (A) with actual field examples (B, C)

A – SSDS resulting, following the numerical modelling, from the passage of a seismic S-wave with a velocity of $2.0 \text{ m} \cdot \text{s}^{-1}$ through a sedimentary succession with 2 m thick stratified porous (15%) sands; **B, C** – seismites at the Rakuti site (SE Latvia) represented by chaotically-deformed layers with numerous small deformations like load casts, pseudonodules, and fragments of broken-up laminae, separated by undeformed layers; this must be ascribed to repeated phases of deformation caused by liquefaction; for details, see [Van Loon et al. \(2016\)](#)

DISCUSSION

Two main issues need some discussion. One is the model itself, together with its relationship with field and experimental data and its potential to predict SSDS development. The second issue concerns the size, geometry and type of the SSDS if a seismically-induced S-wave with a given velocity passes through a sedimentary succession with specific properties.

LIMITATIONS AND ADVANTAGES OF THE MODEL

Although we are aware that the model presented here is relatively simple and cannot be considered as fully developed, we also believe that it provides an interesting insight into the question how seismic S-waves produce SSDS, because all simplifications used for this study can be justified. As mentioned before, the main disadvantage of the modelling procedure presented here is that it addresses only one (vertical) component of only one seismic S-wave (among many). Even though this was our intention, the triggering mechanism for the modelled SSDS can be interpreted in different ways because it can be the resultant vertical velocity of numerous interacting waves. In other words, the velocity used in the model may be considered both as the vertical component of a specific S-wave, as well as the sum of the vertical components of a large number of S-waves. The presented model is therefore specific in that it addresses only a very narrow vertical succession (the “tube”) where S-waves interact with the sediment, while it does not specify its exact distance from the epicentre. Consequently, it is reasonable to assume that the initial conditions assumed in the model are met at some point. Because our main focus is only on the development of SSDS, this assumption is feasible.

The model presented here seems to differ significantly regarding its prediction potential from models that focus at the propagation of seismic waves, or at the processes of liquefaction and fluidisation. Although our model should not be considered as complete or even nearly complete, it is well applicable concerning its main objective to allow the reconstruction of past seismic events; the prediction of the effects of modern seismic events is much less the objective of our model. Due to the reasons listed in the methods section, none of the existing models can be used for this purpose. The urgent need for a numerical method of seismite modelling can be fulfilled by the new approach presented here.

CHARACTERISTICS OF THE SSDS

The geometry of the modelled SSDS is consistent with that of actual seismically-induced and experimentally produced load casts, flame structures, injection structures and



Fig. 4. Comparison of modelled SSDS (A and B) with actual field examples (C–G)

A – SSDS developed after $\sim 0.01 \text{ s}$ following the numerical model when the seismic wave has a velocity of $1.6 \text{ m} \cdot \text{s}^{-1}$; **B** – idem, when the seismic wave velocity has a velocity of $2.6 \text{ m} \cdot \text{s}^{-1}$; **C** – seismite at the Dyburiai site (Lithuania) with strongly deformed load casts of variable size (resulting from different stages of loading), and fragments of broken-up clay laminae (in the uppermost part of the seismite) derived from thin clay laminae affected by liquefaction; for details, see [Belzyt et al. \(2021\)](#); **D** – mushroom-shaped injection structure in a seismite at the Dwasieden site (Rügen Island, NE Germany); for details, see [Pisarska-Jamroży et al. \(2018\)](#); **E** – load casts and flame structures in seismites at the Valmiera site (NE Latvia). The load casts themselves are also deformed, indicating successive phases of deformational activity. Because there are no lithological differences between the sediments within the load casts, the various loading stages must be ascribed to repeated moments of liquefaction. The underlying silty/clayey layer (darker brown) was pressed upwards between the load casts and now forms flame structures. The flame structures still show their original internal lamination and commonly do not intrude the overlying layer with load structures; for details, see [Van Loon et al. \(2016\)](#); **F** – 3D view of deformation structures in a seismite at the Baltmuiza site. The deformed layer contains irregularly-shaped injection structures of sandy silt between load casts and pseudonodules of silty sand that show a wide variety of shapes. The pseudonodules are shown in 3D to have evolved from load casts which sunk into the underlying sandy silt after having become detached from the parent layer; for details, see [Woźniak et al. \(2021\)](#); **G** – seismite with silty injection structures and sandy load casts at the Slinkis site (W Lithuania). The upwards directed injection structures intruded ripple cross-laminated sandy layers, causing the material un between to form load casts. The sharp tops of the injection structures must be described by the current that resulted in the overlying ripple cross-laminated sand; for details, see [Pisarska-Jamroży et al. \(2019a\)](#)

clastic volcanoes. Load casts consist of what have been called “dry sands” in our model (yellowish in Figs. 1–3A, B and 4A), and they are surrounded by denser sands (brownish in Figs. 1–3A, B and 4A) which became liquefied during the modelled earthquake. Field examples of load casts usually contain sands, silty sands or sandy silts (Fig. 3C, E–G; e.g., Oliveira et al., 2011; Van Loon et al., 2016; Brandes et al., 2018; Belzyt et al., 2021). Flame structures, injection structures and clastic volcanoes, contain fluidised, denser sands (brownish in Figs. 1–3A, B and 4A). However, surprising this result may seem, it can be easily justified. During the passage of the S-wave through the sediment column, the wave causes intensive interaction between two layers with different densities, causing dispersal at their mutual boundary plane. This dispersal causes not only reduction of the wave energy, but also a reflection, after which a new, upward-directed wave with some energy appears. This new wave causes the upward movement of the sediment and consequently, the injection of more dense sediment into the lower dense one. Field examples of these SSDS usually show less dense sediments than the sediments that build load casts (e.g., Oliveira et al., 2011; Van Loon et al., 2016; Belzyt et al., 2021). The origin of injection structures such as sand or silt volcanoes is linked to overpressure in the sediment (cf. Van Loon, 2010; Van Loon and Maulik, 2011; Doughty et al., 2014). Such overpressure conditions can be expressed in the shift of seismite depths related to the maxima and minima of the responsible S-waves.

The sizes of the seismically-induced SSDS in our simulations are comparable with those of actual and experimental ones (e.g., Owen, 1996; Moretti et al., 1999; Moretti and Sabato, 2007). Their shape and geometry show a satisfactory similarity with field observations. The SSDS formed in our simulations are of the same type and have the same random distribution as actual seismites. The modelled SSDS do not show any features which are not present in modern and ancient seismites. The depth of their occurrence and the thickness of the deformed layer are consistent with field observations. The numerically simulated SSDS resulting from the model can consequently be considered as very accurate. Moreover, the numerical simulations show the stacks of deformed and undeformed layers (Fig. 2), as well as the wide range of chaotically-distributed SSDS that are well known from field investigations.

CONCLUSIONS

The following five conclusions can be drawn from our numerical modelling of seismites.

- 2D numerical simulations of seismically-induced SSDS results in structures that are similar to actual ones in seismites, which strongly suggests that the main feature responsible for the origination of seismically-induced SSDS is the shear strength related to the vertical velocity component of the seismic wave.
- The sediment compaction is related to initial sediment properties (particularly porosity) and the pressure exerted by the trigger mechanism, described in terms of the velocity of the seismic wave. The more pore water is present in the modelled sediment, the more susceptible to mobilization – and thus to more compaction – it becomes during propagation of the S-wave. With increasing porosity, the size of the developing SSDS increases. The higher the porosity of sediments is, the more complex the geometry of the SSDS becomes.
- The modelled size, geometry and type of the SSDS are linked only slightly to the velocity of the S-wave. However, the S-wave velocity influences the depth at which the seismite originates: the higher the wave velocity is, the deeper the resulting seismite can occur. The geometry and size of the modelled SSDS are consistent with actual and experimentally-produced seismic SSDS such as load casts, flame structures, injection structures and clastic volcanoes.
- The modelled shift in seismite depth can be related to the S-wave maxima and minima, and therefore to the propagation direction of the wave. These shifts also express overpressure conditions in the sediment.
- All results are consistent with previous studies addressing the liquefaction process. In combination with the compliance of the modelled seismites with field data, this strongly suggests that our model is accurate and can serve as a basis for the further development of more worked out models for the recognition of the various characteristics of ancient seismic events.

Acknowledgements. The study was supported by grants from the Polish National Science Center (no. 2015/19/B/ST10/00661 (GREBAL project) and 2019/33/N/ST10/00095). Helpful remarks on the first version by an Anonymous Reviewer and M. Moretti are appreciated.

REFERENCES

- Alfaro, P., Moretti, M., Soria, J.M., 1997. Soft-sediment deformation structures induced by earthquakes (seismites) in Pliocene lacustrine deposits (Guadix-Baza Basin, central Betic Cordillera). *Eclogae Geologicae Helvetiae*, **90**: 531–540.
- Allen, J.R.L., 1982. Sedimentary structures: their character and physical basis. *Developments in Sedimentology*, **30B**.
- Amsden, A., Ruppel, H., Hirt, C., 1980. SALE: A simplified ALE computer program for fluid flow at all speeds. Los Alamos National Laboratories Report, LA-8095.
- Andrus, R.D., Stokoe K.H., 1997. Liquefaction resistance based on shear wave velocity. National Center for Earthquake Engineering Research (Salt Lake City) Report, 0022.
- Atkinson, G.M., Eeri, M., Liam, Finn, W.D., Charlwood, R.G., 1984. Simple computation of liquefaction probability for seismic hazard applications. *Earthquake Spectra*, **1**: 107–123.
- Belzyt, S., Pisarska-Jamroży, M., Bitinas, A., Woronko, B., Phillips, E.R., Piotrowski, J.A., Jusienė, A., 2021. Repetitive soft-sediment deformation by seismicity-induced liquefaction in north-western Lithuania. *Sedimentology*, **68**: 3033–3056.
- Brandes, Ch., Steffen, H., Sandersen, P.B.E., Wu, P., Winsemann, J., 2018. Glacially induced faulting along the NW segment of the Sorgenfrei-Tornquist Zone, northern Denmark: implications for neotectonics and lateglacial fault-bound basin formation. *Quaternary Science Reviews*, **189**: 149–168.

- Boulanger, R., Ziotopoulou, K., 2017.** PM4sand version 3.1: a sand plasticity model for earthquake engineering applications. Report UC Davis Center for Geotechnical Modeling Report, UCD/CGM-17/01.
- Collins, G.S., Melosh, H.J., Ivanov, B.A., 2004.** Modeling damage and deformation in impact simulations. *Meteoritics & Planetary Science*, **39**: 217–231.
- Davison, T.M., Collins, G.S., Elbeshausen, D., Wünnemann, K., Kearley, A., 2011.** Numerical modeling of oblique hypervelocity impacts on strong ductile targets. *Meteoritics & Planetary Science*, **46**: 1510–1524.
- Doughty, M., Eyles, N., Eyles, C.H., Wallace, K., Boyce, J.I., 2014.** Lake sediments as natural seismographs: earthquake-related deformations (seismites) in central Canadian lakes. *Sedimentary Geology*, **313**: 45–67.
- Galli, P., 2000.** New empirical relationships between magnitude and distance for liquefaction. *Tectonophysics*, **324**: 169–187.
- Hilbert-Wolf, H.L., Simpson, E.L., Simpson, W.S., Tindall, S.E., Wizevich, M.C., 2009.** Insights into syndepositional fault movement in a foreland basin; trends in seismites of Upper Cretaceous Wahweap Formation, Kaiparowits Basin, Utah, U.S.A. *Basin Research*, **21**: 856–871.
- Hoffman, G., Reichert, K., 2012.** Soft-sediment deformation of Late Pleistocene sediments along the southwestern coast of the Baltic Sea (NE Germany). *International Journal of Earth Sciences*, **101**: 351–363.
- Jeffereis, M., Been, K., 2015.** Soil Liquefaction – a Critical State Approach. CRC Press.
- Li, C., Liu, J., Sun, Y., 2020.** Optimal third-order symplectic integration modeling of seismic acoustic wave propagation. *Bulletin of the Seismological Society of America*, **110**: 754–762.
- Marco, S., Agnon, A., 1995.** High-resolution stratigraphy reveals repeated earthquake faulting in the Masada Fault Zone, Dead Sea Transform. *Tectonophysics*, **408**: 101–112.
- Meada, T., Takemura, S., Furumura, T., 2017.** OpenSWPC: an open source integrated parallel simulation code for modeling seismic wave propagation in 3D heterogeneous viscoelastic media. *Earth, Planets and Space*, **69**: 1–20.
- Miljković, K., Collins, G.S., Patel, M.R., Chapman, D., Proud, W., 2012.** High-velocity impacts in porous solar system materials. *AIP Conference Proceedings*, **1426**: 871–874.
- Moretti, M., Sabato, L., 2007.** Recognition of trigger mechanisms for soft-sediment deformation in the Pleistocene lacustrine deposits of the Santi Arcangelo Basin (Southern Italy): Seismic shock vs. overloading. *Sedimentary Geology*, **196**: 31–45.
- Moretti, M., Ronchi, A., 2011.** Liquefaction features interpreted as seismites in the Pleistocene fluvio-lacustrine deposits of the Neuquén Basin (Northern Patagonia). *Sedimentary Geology*, **235**: 200–209.
- Moretti, M., Alfaro, P., Caselles, O., Canas, J.A., 1999.** Modelling seismites with a digital shaking table. *Tectonophysics*, **304**: 369–383.
- Obermeier, S.F., 1996.** Use of liquefaction-induced features for paleoseismic analysis – an overview of how seismic liquefaction features can be distinguished from other features and how their regional distribution and properties of source sediment can be used to infer the location and strength of Holocene paleo-earthquakes. *Engineering Geology*, **44**: 1–76.
- Obermeier, S.F., 2009.** Using liquefaction-induced and other soft-sediment features for paleoseismic analysis. In: *Paleoseismology* (ed. J.P. McCalpin): 487–564. Elsevier, New York.
- Obermeier, S.F., Jacobson, R.B., Smoot, J.P., Weems, R.E., Gohn, G.S., Monroe, J.E., Powars, D.S., 1990.** Earthquake-induced liquefaction features in the coastal setting of South Carolina and in the fluvial setting of the New Madrid seismic zone. U.S.G.S. Professional Paper, **1504**.
- Oliveira, C.M.M., Hodgson, D.M., Flint, S.S., 2011.** Distribution of soft-sediment deformation structures in clinoform successions of the Permian Ecca Group, Karoo Basin, South Africa. *Sedimentary Geology*, **235**: 314–330.
- Owen, G., 1996.** Experimental soft-sediment deformation: structures formed by the liquefaction of unconsolidated sands and some ancient examples. *Sedimentology*, **43**: 279–293.
- Owen, G., Moretti, M., 2011.** Identifying triggers for liquefaction-induced soft-sediment deformation in sands. *Sedimentary Geology*, **235**: 141–147.
- Peng, P., Wang, L., 2019.** 3DMRT: a computer package for 3D model-based seismic wave propagation. *Seismological Research Letters*, **90**: 2039–2045.
- Pierazzo, E., Artemieva, N., Asphaug, N., Baldwin, E., Cazamias, E.C., Coker, R., Collins, G.S., Crawford, D.A., Davison, T., Elbeshausen, D., Holsapple, K.A., Housen, K.R., Korycansky, D.G., Wünnemann, K., 2008.** Validation of numerical codes for impact and explosion cratering: Impacts on strengthless and metal targets. *Meteoritics & Planetary Science*, **43**: 1917–1938.
- Pisarska-Jamroży, M., Woźniak, P.P., 2019.** Debris flow and glacioisostatic-induced soft-sediment deformation structures in a Pleistocene glaciolacustrine fan: the southern Baltic Sea coast, Poland. *Geomorphology*, **326**: 225–238.
- Pisarska-Jamroży, M., Belzyt, S., Börner, A., Hoffmann, G., Hüneke, H., Kenzler, M., Obst, K., Rother, H., Van Loon, A.J., 2018.** Evidence from seismites for glacio-isostatically induced crustal faulting in front of an advancing land-ice mass (Rügen Island, SW Baltic Sea). *Tectonophysics*, **745**: 338–348.
- Pisarska-Jamroży, M., Belzyt, S., Bitinas, A., Jusienė, A., Woronko, B., 2019a.** Seismic shocks, periglacial conditions and glaciectonics as causes of the deformation of a Pleistocene meandering river succession in central Lithuania. *Baltica*, **32**: 63–77.
- Pisarska-Jamroży, M., Van Loon, A.J., Mleczak, M., Roman, M., 2019b.** Enigmatic gravity-flow deposits at Ujście (western Poland), triggered by earthquakes (as evidenced by seismites) caused by Saalian glacioisostatic crustal rebound. *Geomorphology*, **326**: 239–251.
- Pisarska-Jamroży, M., Woronko, B., Bujak, Ł., Bitinas, A., Belzyt, S., Mleczak, M., 2019c.** Large-scale deformation structures characterize glaciolacustrine kame sediments – a new kame-investigation approach. Abstract book INQUA Congress 2019 (Dublin) O-1128.
- Rahman, M., Lo, S., 2014.** Undrained behavior of sand-fines mixtures and their state parameters. *Journal of Geotechnical and Geoenvironmental Engineering*, **140**: 04014036.
- Rahman, M., Asce, M., Nguyen, H.B.K., Fourie, A.B., Kuhn, M.R., 2020.** Critical state soil mechanics for cyclic liquefaction and postliquefaction behavior: DEM study. *Journal of Geotechnical and Geoenvironmental Engineering*, **147**: 04020166.
- Rodríguez-Pascua, M.A., Calvo, J.P., De Vicente, G., Gomez Gras, D., 2000.** Seismites in lacustrine sediments of the Prebetic Zone, SE Spain, and their use as indicators of earthquake magnitudes during the late Miocene. *Sedimentary Geology*, **135**: 117–135.
- Rossetti, D.F., 1999.** Soft-sediment deformation structures in late Albian to Cenomanian deposits, Sao Luis Basin, northern Brazil: evidence for palaeoseismicity. *Sedimentology*, **46**: 1065–1081.
- Rossetti, D.F., Bezerra, F.H.R., Goes, A.N., Neves, B.B.B., 2011.** Sediment deformation in Miocene and post-Miocene strata, Northeastern Brazil: Evidence for paleoseismicity in a passive margin. *Sedimentary Geology*, **235**: 172–187.
- Seed, H.B., Idris, I.M., 1971.** Simplified procedure for evaluating soil liquefaction potential. *Journal of Soil Mechanics and Foundations Division*, **97**: 1249–1273.
- Seilacher, A., 1969.** Fault-graded beds interpreted as seismites. *Sedimentology*, **13**: 15–159.
- Vaid, Y.P., Thomas, J., 1995.** Liquefaction and postliquefaction behavior of sand. *Journal of Geotechnical Engineering*, **121**: 1321–1337.
- Van Loon, A.J., 2010.** Sedimentary volcanoes: overview and implications for the definition of a “volcano” on Earth. *GSA Special Paper*, **470**: 31–41.

- Van Loon, A.J., Maulik, P., 2011.** Abraded sand volcanoes as a tool for recognizing paleo-earthquakes, with examples from the Cisuralian Talchir Formation near Angul (Orissa, eastern India). *Sedimentary Geology*, **238**: 145–155.
- Van Loon, A.J., Pisarska-Jamroży, M., 2014.** Sedimentological evidence of Pleistocene earthquakes in NW Poland induced by glacioisostatic rebound. *Sedimentary Geology*, **300**: 1–10.
- Van Loon, A.J., Pisarska-Jamroży, M., Nartišs, M., Krievāns, M., Soms, J., 2016.** Seismites resulting from high-frequency, high-magnitude earthquakes in Latvia caused by Late Glacial glacio-isostatic uplift. *Journal of Palaeogeography*, **5**: 363–380.
- Van Loon, A.J., Pisarska-Jamroży, M., Woronko, B., 2020.** Sedimentological distinction in glacial sediments between load casts induced by periglacial processes from those induced by seismic shocks. *Geological Quarterly*, **64** (3): 626–640.
- Vanneste, K., Meghraoui, M., Camelbeeck, T., 1999.** Late Quaternary earthquake-related soft-sediment deformation along the Belgian portion of the Feldbiss Fault, Lower Rhine Graben system. *Tectonophysics*, **309**: 57–79.
- Wheeler, R.L., 2002.** Distinguishing seismic from nonseismic soft-sediment structures: criteria from seismic-hazard analysis. *GSA Special Paper*, **359**: 1–11.
- Woźniak, P.P., Belzyt, S., Pisarska-Jamroży, M., Woronko, B., Lamsters, K., Nartišs, M., Bitinas, A. 2021.** Liquefaction and re-liquefaction of sediments induced by uneven loading and glacial earthquakes: implications of results from the Latvian Baltic Sea coast. *Sedimentary Geology*, **421**: 105944.
- Wünnemann, K., Colling, G.S., Melosh, H., 2006.** A strain-based porosity model for use in hydrocode simulations of impacts and implications for transient crater growth in porous target. *Icarus*, **180**: 514–527.
- Youd, T.L., Idriss, I.M., 2001.** Liquefaction resistance of soil: summary report from the 1996 NCEER and 1998 NCEER/NFS workshop on evaluation of liquefaction resistance of soil. *Journal of Geotechnical and Geoenvironmental Engineering*, **127**: 1275–1285.